PHYSICAL REVIEW B VOLUME 33, NUMBER 2 15 JANUARY 1986

Self-consistent calculation of electron-density profiles at strongly charged jellium surfaces

P. Gies and R. R. Gerhardts
Institut für Theoretische Physik, Freie Universität Berlin, D-1000 Berlin 33, Federal Republic of Germany
(Received 3 June 1985)

We present a self-consistent calculation of the electron distribution at a jellium surface in a strong static electric field, based on the Hohenberg-Kohn-Sham theory in the local-density approximation. For different metallic densities $r_s = 2,3,4,5$ and the wide range of surface-charge densities accessible to experiments in electrolytic cells, we calculate suitable moments characterizing the electron-density profile, and give results for the center of mass and spread of the induced charge density, which are related to static and optical response properties, respectively. Our self-consistent results differ remarkably from previous results based on other methods and from model assumptions previously made in order to explain properties of charged surfaces.

I. INTRODUCTION

The purpose of this paper is to report the first[1] (to our knowledge) fully-self-consistent quantum-mechanical calculations of the electronic density profile of a jellium-metal surface in a strong static electric field F, and to present numerical results for two length parameters, which roughly characterize the shape of the induced charge-density profile, namely its mean position z_0 and its width λ. Whereas z_0 governs static response properties such as the surface contribution to the capacitance or the image force on a point charge outside the metal, the width λ is essentially a screening length of the applied static field F, and plays an important role for the optical response of the charged metal surface.

Our calculations are based on the Hohenberg-Kohn-Sham formalism[2] in the local-density approximation and extend the pioneering work of Lang and Kohn[3-5] to charged surfaces far beyond the linear-response regime. This extension is necessary for an understanding of metal surfaces under very strong electric fields, e.g., of the order of 1 V/Å, as can easily be reached at electrode surfaces in electrolytic cells. Indeed, optical techniques such as electroreflectance,[6,7] excitation of surface plasmons,[8] or ellipsometry[9] yield signals which depend on the applied static field in a strongly nonlinear way and change completely, if the field is reversed. This indicates the inadequacy of a linear-response treatment.

Previous work on charged jellium surfaces outside the linear-response regime used either an *ad hoc*, non-self-consistent model ansatz for the effective one-electron potential,[10] or a restricted set of trial functions for the electron density, avoiding the solution of Schrödinger's equation altogether.[11-13] A fully-self-consistent calculation (in the spirit of Lang and Kohn) of characteristic properties of strongly charged jellium surfaces has, to the best of our knowledge, not been presented before.

We should, however, mention in this context the work of Ho, Harmon, and Liu[14] on the electronic structure of the Ag(110) surface in an applied electric field. In order to explain the polarization anisotropy of the normal-incidence electroreflectance of the (110) faces of noble metals, these authors calculated within the self-consistent pseudopotential method[15] the Ag(110)-projected band structure and emphasized the importance of unoccupied surface states, which were found at energy levels depending strongly on the applied electric fields. The results of Ho *et al.* are typical for silver and, probably, the (110) faces of other noble metals. The induced charge density averaged parallel to the surface was calculated by Ho *et al.* for a certain strength of the applied field, and resembles corresponding jellium results. A quantitative agreement can, of course, not be expected, since the periodic lattice potential and, therefore, band-structure effects and surface states are not taken into account in the jellium model.

The intention of the present work is complementary to that of Ref. 14. Using the jellium model as a simple but reasonable model for free-electron metals, we investigate in a systematic manner the dependence of characteristic features of the surface-electron distribution on an applied electric field, covering a wide range of field strengths and the whole range of metallic densities. A reliable knowledge of the electron-density profile at the surface is, for instance, important in the context of nonlocal optics,[16] which investigates typical deviations from the classical Fresnel optics occurring for p-polarized light, but not for normal incidence. The special optical anisotropy of noble-metal (110) faces addressed by Ho *et al.*[14] is, on the other hand, beyond the scope of our model assumptions.

In the past, more or less sophisticated step models for the electron-density profile have been employed in order to understand or evaluate optical data on charged surfaces.[7,9,16,17] In Fig. 1(a) we sketch the simplest step model, which has been used by Chao and Costa[9] to evaluate their ellipsometry data on positively charged Au surfaces in the framework of classical optics. Recently, Kempa[17] pointed out that nonlocal optics[16] should be used instead, and evaluated the same data with the model sketched in Fig. 1(b), taking into account the diffuseness of the uncharged surface. Whereas classical optics suggests[9] that the width λ of the induced charge density depends linearly on the external field F, Kempa's result[17] for λ is essentially independent of F, and of the order

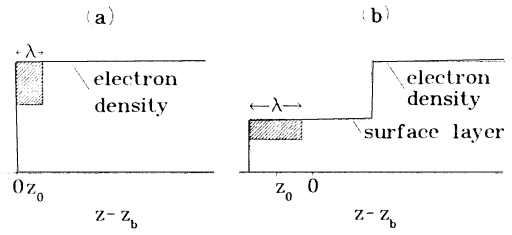

FIG. 1. Step models of the electron density at a charged metal surface (induced charge is hatched). The center of mass z_0 of the induced charge is inside the jellium ($z_0>0$) for model (a), but outside ($z_0<0$) for model (b).

$\lambda\sim 2.5$–3 Å, which is consistent with the width of the self-consistently calculated profile of induced charge in the linear-response regime.[5] Similar step models have also been used to explain electroreflectance data.[7,16]

Two problems become apparent with such step models. First, there is a trivial linear relationship between the width λ of the induced charge-density profile and its center of mass z_0. This relationship is an artifact of the model and does not hold for the self-consistent calculations. Second, the choice of parameters for models with several steps involves some arbitrariness and is, in view of the crudeness of the model, hard to justify. To avoid such model assumptions, or eventually to justify them, we have performed the self-consistent calculations.

The paper is organized as follows. In Sec. II we formulate the Hohenberg-Kohn-Sham equations in the local-density approximation for a finite jellium slab in a strong static external electric field. In Sec. III we present and discuss our results and compare them with previous work. Section IV contains a brief summary, and a description of the numerical techniques is given in the Appendix.

II. THE MODEL

For reasons of computational convenience, we consider a thin plane metal slab within the jellium model, i.e., we replace the ions by a uniform background of positive charge, and assume vacuum on both sides of the slab. We take the width of the slab to be so large, actually of the order of 10–20 Å, that for zero total charge our results for effective potential and electron density in the surface region agree well with the results obtained by Lang and Kohn[3] for the surface of a metallic half-space with the same background density.

The physical situation we have in mind is an electrode (the slab) in an electrolyte, kept at constant potential on both sides of the slab, so that a strong electric field, which induces surface charges in the slab, is present only in a thin transition region (~Helmholtz layer) of a few angstroms thickness at the slab's surfaces. Even for negative surface charge we will assume that the potential energy of electrons in the electrolyte region is larger than the Fermi level in the slab, so that the electron density is negligibly small in the electrolyte region, and tunneling and field emission do not occur. The capacity of a metal-electrolyte interface was recently discussed by Feldman *et al.*[13] within a detailed model for the interaction between metal and electrolyte. Here we are only interested in the metal side and simulate the situation by a simple model which does not consider the electrolyte explicitly. We assume infinite potential barriers, located symmetrically on both sides of the slab and sufficiently far away, so that the electron density is negligibly small in the neighborhood of the barriers. This model, schematically shown in Fig. 2, allows us to treat the effect of a constant external electric field of either sign in terms of stationary states. Due to its symmetry, numerical calculations can be restricted to the layer between the left barrier at $z=-a$ and the middle of the slab at $z=b$, where the z direction is taken to be perpendicular to the slab, and the left edge of the positive background is at $z=0$.

We use the following notations: The jellium density n_+ is related to the Wigner-Seitz radius (in units of $a_0=\hbar^2/me^2\approx 0.529$ Å, where m is the electron mass)

$$r_s=(\tfrac{1}{3}4\pi n_+ a_0^3)^{-1/3}\,, \tag{2.1}$$

$n(z)$ denotes the electron density, and

$$\rho(z)=-e[n(z)-n_+\Theta(z)\Theta(2b-z)]\,,$$
$$\Theta(z)=\begin{cases}1, & z>0\\ 0, & z<0\end{cases} \tag{2.2}$$

the total charge density. A static electric field F applied perpendicular to the slab is characterized by the induced surface charge density

$$\sigma=-F/4\pi=\int_{-a}^{b} dz\,\rho(z)=\int_{-a}^{b} dz\,\delta\rho(z)\,, \tag{2.3}$$

where $\delta\rho(z)$ is the induced charge density. The electrostatic potential energy $\phi(z)$ obeys Poisson's equation,

$$\frac{d^2}{dz^2}\phi(z)=4\pi e\rho(z)\,. \tag{2.4}$$

Since $n(z)$ and $\phi(z)$ are symmetrical with respect to b, we obtain, from (2.4),

$$\frac{d}{dz}\phi(z)=-4\pi e\sigma+4\pi e\int_{-a}^{z} dz'\rho(z') \tag{2.5}$$

and, integrating by parts,

$$\phi(z)-\phi(b)=4\pi e\left[D(\sigma)-z\sigma+\int_{-a}^{z} dz'(z-z')\rho(z')\right]\,. \tag{2.6}$$

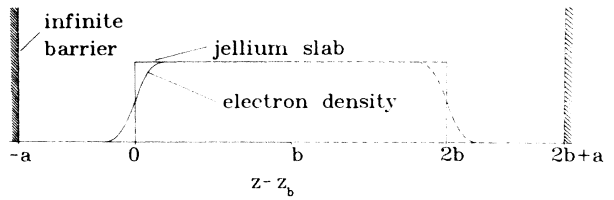

FIG. 2. Model system with a jellium slab of width $2b$ and infinite potential barriers located symmetrically at $z=-a$ and $z=2b+a$.

The electric dipole moment (per unit area)

$$D(\sigma)=\int_{-a}^{b} dz\, z\rho(z)=D(0)+\sigma z_0(\sigma) \tag{2.7}$$

can be expressed in terms of the dipole moment $D(0)$ of the neutral surface and of the center of mass

$$z_0(\sigma)=\frac{1}{\sigma}\int_{-a}^{b} dz\, z\,\delta\rho(z) \tag{2.8}$$

of the induced charges.

A sum rule derived by Budd and Vannimenus[18] implies that one part of the induced dipole moment $D(\sigma)-D(0)$ is related trivially to the induced surface charge density σ. The total electrostatic force exerted by the induced charges on the left infinite barrier (representing the electrolyte) sums to $2\pi\sigma^2$. It must be equal and opposite to the force acting on the jellium between 0 and b, which can be calculated from the induced electric field [Eq. (2.5)]. The result is[18]

$$\tfrac{1}{2}\sigma^2=en_+\int_0^b dz\, z\,\delta\rho(z)\ . \tag{2.9}$$

This implies that the center of mass of the induced charges can be calculated alternatively from the equation

$$z_0(\sigma)=\frac{\sigma}{2en_+}+\frac{1}{\sigma}\int_{-a}^{0} dz\, z\,\delta\rho(z)\ . \tag{2.10}$$

In the framework of the density-functional formalism,[2] the exact ground-state electron density of our model system is given as the self-consistent solution of the equations

$$n(z)=\frac{m}{\pi\hbar^2}\sum_{\nu}(\epsilon_F-\epsilon_\nu)\Theta(\epsilon_F-\epsilon_\nu)\,|\,\psi_\nu(z)\,|^2\ , \tag{2.11}$$

$$-\frac{\hbar^2}{2m}\frac{d^2}{dz^2}\psi_\nu(z)+(v_{\rm eff}[n;z]-\epsilon_\nu)\psi_\nu(z)=0\ , \tag{2.12}$$

where ϵ_ν and ψ_ν are, respectively, the energy eigenvalues and normalized eigenfunctions of an electron in the one-dimensional effective potential $v_{\rm eff}$ which, in turn, is a functional of the electron density $n(z)$. With suitably normalized plane waves for the (x,y)-dependent parts of the wave functions, $n(z)$ can be calculated for given $v_{\rm eff}$ from Eq. (2.11), where the Fermi energy ϵ_F is determined by Eq. (2.3), which can be written as

$$\frac{m}{2\pi\hbar^2}\sum_{\epsilon_\nu<\epsilon_F}(\epsilon_F-\epsilon_\nu)=bn_+-\frac{\sigma}{e}\ . \tag{2.13}$$

The effective potential $v_{\rm eff}[n;z]$ is the sum of the electrostatic contribution $\phi(z)$ given by Eq. (2.6) and an exchange and correlation part. Following the work of Lang and Kohn,[3] we use the local-density approximation of the latter,

$$v_{\rm eff}[n;z]=\phi(z)+\mu_{\rm xc}(n(z))\ , \tag{2.14}$$

with Wigner's expression for the correlation energy,[3] so that

$$\mu_{\rm xc}(n(z))=-\frac{e^2}{a_0}\left[\frac{0.611}{r_s(z)}+0.147\frac{4r_s(z)+7.8}{[r_s(z)+7.8]^2}\right]\ , \tag{2.15}$$

where $r_s(z)$ is obtained from Eq. (2.1) if n_+ is replaced by the local electron density $n(z)$.

Since direct iteration does not converge, we used for the numerical calculations a procedure similar to that described by Lang and Kohn.[3] Some details of our method are given in the Appendix. About five to eight iteration steps were sufficient to obtain the desired accuracy.

III. RESULTS AND DISCUSSION

A. Density profile of a charged surface

Figure 3 shows typical results for the self-consistent effective potential $v_{\rm eff}[n;z]$ and electron density $n(z)$ of a neutral (curves b and b', respectively) and two oppositely charged surfaces. The uniform positive background has a slab thickness of 16 Å and a density $n_+=5.967\times10^{22}$ cm^{-3}, corresponding to $r_s=3$. The results of our slab calculation for the neutral system agree within numerical accuracy with the values tabulated by Lang and Kohn[3] for the metallic half-space. Slight differences are expected near the center of the slab, where, by symmetry, the slope of our $n(z)$ must vanish, and immediately at the infinite barrier, where our effective potential bends upwards. This effect nicely visualizes how the infinite barrier disturbs the electron system and is understood as follows. At some distance from the infinite barrier the electron density is already very small, $n(z)/n_+\sim10^{-6}$, so that $\phi(z)$ has reached its asymptotic value. However, $\mu_{\rm xc}(n(z))\sim-n(z)^{1/3}$, being of the order of 10^{-2}, varies still noticeably on the scale of Fig. 3 and is forced to vanish at the barrier. This leads to the upward bending of the effective potential, but has negligible effect on the density profile. The magnitude of this infinite-barrier effect de-

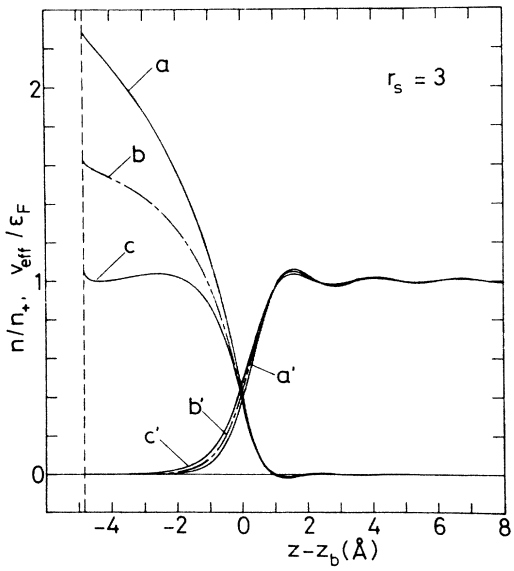

FIG. 3. Self-consistent effective potential of (a) a positively charged, (b) neutral, and (c) negatively charged surface, in units of the Fermi energy ϵ_F, and the corresponding electron density in units of n_+ for $r_s=3$. The induced surface charge density is $\pm4.77\times10^{-3}$ $e/$Å^2, the slab width 16 Å, and the distance between the jellium edge and the infinite barrier 4.8 Å.

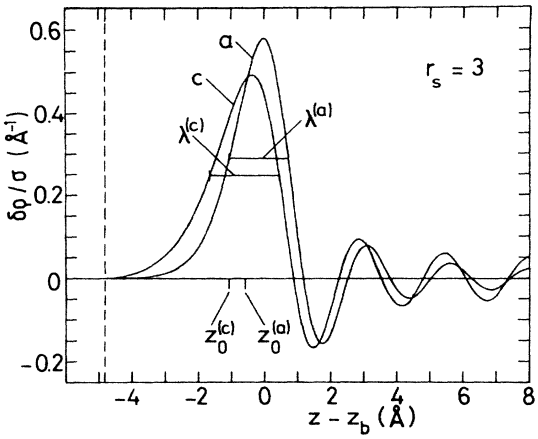

FIG. 4. Normalized self-consistent induced charge density for (a) a positively and (c) a negatively charged surface (same parameters as in Fig. 3). Center of mass z_0 and spread λ are indicated.

creases exponentially with increasing distance between barrier and slab. Figure 3 also shows results for a positively (curves a and a') and a negatively (curves c and c') charged surface with $\sigma=\pm 4.77\times 10^{-3}\ e/\text{Å}^2$, corresponding to an external electric field $F(-a)=\mp 0.861$ V/Å, which is of the order of the fields occurring at electrochemical interfaces.[9] As a function of σ, the density profile changes its form, the largest effects occurring in the low-density tail. This is easily understood, since only the electron wave functions with high energy extend far outside the jellium and thus are strongly affected by the external electric field. Inside the metal the electron density is less disturbed by the field, since, according to Eq. (2.11), these wave functions contribute little. For positive surface charge, electrons are removed from the tail region, the density profile (curve a') becomes steeper, and the Friedel oscillations become more pronounced. For negative surface charge, electrons are pulled into the tail region, the density profile (curve c') becomes smoother, and the Friedel oscillations are diminished.

In Fig. 4 we plot the normalized induced charge densities $\delta\rho/\sigma$, corresponding to Fig. 3. Also indicated are the mean positions $z_0(\sigma)$ of the induced charges, defined by Eq. (2.8). The results are similar to those obtained by Lang and Kohn,[4,5] for a weak external electric field, but the deviations from the linear-response result, which in this plot yields only a single curve for all values of σ, are clearly seen.

B. Position and spread of induced charges

We characterize the induced charge-density profile by its center of mass $z_0(\sigma)$ [Eq. (2.8)] and, since it is clearly dominated by a single peak followed by weak oscillations, by the full width at half maximum $\lambda(\sigma)$ of that peak.

The physical importance of z_0, determining the position of the image plane for an external point charge in front of the surface,[5,10] or the metal contribution to the capacity of a parallel-plate condenser,[5,10] or a metal-electrolyte interface,[12,13] has been appreciated by many authors.[4,5,10,12,13]

In Fig. 5 our results for $z_0(\sigma)$ (pluses), calculated with Eq. (2.8), are shown together with those of Theophilou and Modinos[10] (curve a) and of Schmickler and Henderson[12] (curve b). The value $r_s=3$ corresponds to the density of s-p electrons in gold. This facilitates comparison with the experiments of Chao and Costa,[9] who reported positive surface charges up to $5\times 10^{-2}\ e/\text{Å}^2$. Note that $z_0(\sigma)$ is negative, i.e., it lies in front of the jellium edge for moderate surface charges.

Our results are in agreement with those of Schmickler and Henderson[12] in the regime of relatively small σ, whereas for larger positive and negative values of σ systematic differences occur. Apparently, the restricted ansatz for the density profile $n(z)$ used in Ref. 12 is not flexible enough to account for the considerable modifications of the fully-self-consistent profile in strong external electric fields. In particular, it does not contain the following physical effect, which limits our calculations for large negative values of σ. With increasing negative surface charge, the maximum value of the effective potential decreases, and eventually becomes smaller than the Fermi energy, so that electrons sweep out of the slab and are bounded by the infinite barrier (our simplified model of repulsion by the electrolyte) only. We exclude this situation from consideration and require the electron density to be negligibly small in the neighborhood of the barrier. For $r_s=3$, this limits our calculations to a surface charge density $\sigma \gtrsim -5\times 10^{-3}\ e/\text{Å}^2 = -0.08$ C/m^2, corresponding to an electric field of 0.9 V/Å.

Curve a of Fig. 5 indicates a result obtained by Theophilou and Modinos[10] from an "approximate semi-self-consistent calculation," which determines induced charge and induced potential change self-consistently, but uses a non-self-consistent, *ad hoc* model potential to describe the

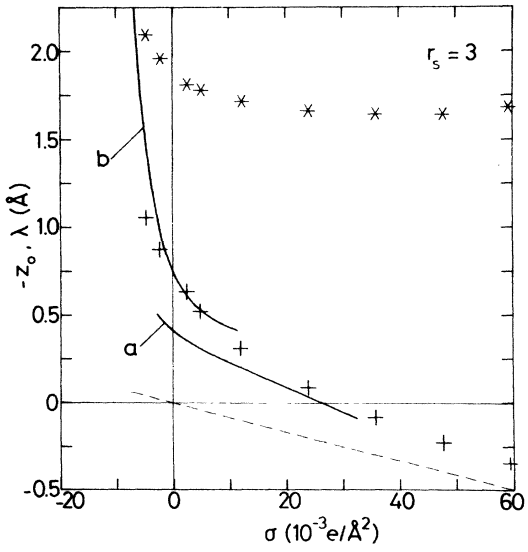

FIG. 5. Our result for the center of mass z_0 (+) and spread λ (*) of the induced charge density as a function of surface charge density σ. The dashed straight line gives the asymptotic behavior of z_0 for large σ. Curves a and b are results for z_0 from Refs. 10 and 12, respectively.

neutral jellium surface. For different model potentials different $z_0(\sigma)$ curves were obtained,[10] and curve *a* shows that which compares most favorably with our self-consistent results. According to Theophilou and Modinos, the essentially linear dependence of z_0 on σ indicates that the electron-density profiles of the charged surfaces are related to the profile of the neutral surface by essentially a rigid displacement. This argument is, even for a jellium half-space ($b \to \infty$), not quite correct: A rigid shift of the electron density by a distance s produces the surface charge density $\sigma = en_+ s$, and the center of mass of the induced charge is just $z_0(\sigma) = \frac{1}{2}s = \sigma/(2n_+ e)$, which is indicated in Fig. 5 by the dashed straight line. The numerical results, on the other hand, indicate that only for large positive values of σ does an essentially rigid displacement of the charge-density profile remain. In this limit the integral in the Budd-Vannimenus sum rule, Eq. (2.10), which collects only contributions from the vacuum region, becomes independent of σ, so that $z_0(\sigma)$ approaches asymptotically ($\sim 1/\sigma$) the dashed straight line in Fig. 5. Apparently, the pluses in Fig. 5 show exactly this behavior. The linear part of curve *a*, however, cannot be explained by a rigid shift of the density profile, since it does not coincide with the dashed straight line. The poor agreement of curve *a* with our results demonstrates the importance of using a consistent approximation scheme, which treats the "induced" and the "ground-state" electron density, i.e., the electron density with and without static electric field, on equal footing.

As mentioned in the Introduction, optical experiments on a positively charged metal surface are usually interpreted in terms of a surface layer of reduced electron density.[7,9,16,17] The optical properties of the charged surface depend on the width of this layer, which corresponds to the spread of the induced charges in our calculation, i.e., the full width at half maximum λ of the induced charge density $\delta\rho(z)$. Since the induced charges screen the electric field, this λ can also be interpreted as static screening length. Our result for λ given by the asterisks in Fig. 5 demonstrates that it depends only weakly on σ and becomes minimum near $\sigma = 0.04\ e/\text{Å}^2$. Neither a linear relationship between $\lambda(\sigma)$ and $z_0(\sigma)$, as implied by the step models of Fig. 1, nor a monotonic increase of λ with increasing values of $|\sigma|$, as would result from a rigid displacement of the electron profile, is compatible with our result.

TABLE I. Various lengths (in Å) characterizing the density profiles: Center of mass z_0 and spread λ of the induced charge-density profile, classical turning point z_t, and the moments d and $l^{(0)}$ of the electron-density profile, for different values of the background density (given by r_s) and the surface charge σ (in units of $e/\text{Å}^2 = 16.02\ \text{C/m}^2$).

r_s	σ ($\times 10^3$)	z_0[a]	z_0[b]	z_t	λ	d	$l^{(0)}$
2	15.10	−0.435	−0.447	−0.782	1.427	0.389	0.207
2	10.07	−0.485	−0.499	−0.897	1.460	0.405	0.214
2	5.03	−0.541	−0.557	−1.052	1.501	0.425	0.221
2	0.00			−1.297		0.448	0.230
2	−5.03	−0.671	−0.695	−1.947	1.607	0.475	0.239
3	59.67	0.357	0.359	0.408	1.685	0.366	0.188
3	47.73	0.228	0.227	0.211	1.658	0.372	0.191
3	35.80	0.084	0.082	0.016	1.649	0.383	0.195
3	23.87	−0.086	−0.089	−0.200	1.666	0.403	0.203
3	11.93	−0.310	−0.311	−0.500	1.723	0.444	0.221
3	4.77	−0.522	−0.511	−0.778	1.785	0.490	0.240
3	2.39	−0.633	−0.612	−0.907	1.813	0.514	0.249
3	0.00			−1.062		0.548	0.262
3	−2.39	−0.874	−0.855	−1.280	1.962	0.596	0.278
3	−4.77	−1.056	−1.041	−4.510	2.101	0.666	0.298
4	2.52	−0.488	−0.478	−0.671	2.135	0.574	0.265
4	1.26	−0.568	−0.557	−0.779	2.171	0.598	0.275
4	0.00			−0.907		0.628	0.287
4	−1.26	−0.772	−0.760	−1.063	2.278	0.668	0.301
4	−2.52	−0.914	−0.901	−1.269	2.361	0.724	0.320
4	−3.78	−1.112	−1.094	−4.013	2.487	0.809	0.343
5	1.55	−0.479	−0.456	−0.581	2.413	0.640	0.277
5	0.77	−0.565	−0.538	−0.684	2.445	0.665	0.288
5	0.00			−0.799		0.695	0.300
5	−0.77	−0.773	−0.740	−0.932	2.535	0.734	0.316
5	−1.55	−0.910	−0.875	−1.088	2.603	0.787	0.335

[a] Calculated with Eq. (2.8).
[b] Calculated with Eq. (2.10).

If we define a "penetration depth" of the external electric field as the position (with respect to the jellium edge) where it has been screened to about one-quarter of its vacuum value, it is roughly given by $z_0(\sigma)+\frac{1}{2}\lambda(\sigma)$. For a surface charge density of $\sigma=0.05\ e/\text{Å}^2=80\ \mu\text{C/cm}^2$ and $r_s=3$, this penetration depth is about 1 Å. It is hard to believe that a real metal surface can be stable under such a gigantic charge.

Values of position $z_0(\sigma)$ and spread $\lambda(\sigma)$ of the induced charge density for $r_s=2,3,4,5$ and different surface charges σ are given in Table I. $z_0(\sigma)$ has been calculated by both Eq. (2.8) and (2.10), giving an estimate of the numerical accuracy of the values. Also shown is the "classical turning point" $z_t(\sigma)$, defined as the position at which the effective potential equals the Fermi energy. It is of some importance for tunneling experiments[5] and varies stronger than $z_0(\sigma)$, especially for negative σ values.

C. Shape analysis of density profiles

As we have seen, the electron-density profile of a charged surface is not obtained by a rigid shift from that of a neutral surface, but rather by a deformation which affects especially the tail region (cf. Fig. 3). The shape of the tail region, which is known to be important, e.g., for the optical-response properties of the metal surface,[16,19] can be characterized by the moments

$$l^{(\nu)}=\frac{1}{n_+}\int_{-a}^{s} dz\,(s-z)^{\nu} n(z)\ . \tag{3.1}$$

For $\nu=0,1$, these have the following meaning: The number (per unit area) of spilled-out electrons with respect to the plane $z=s$ is given by $n_+ l^{(0)}$, and the length

$$d=l^{(1)}/l^{(0)} \tag{3.2}$$

gives the center of mass (or dipole length) of the spilled-out electrons with respect to this plane. A rough estimate for the width of the tail region ($z<s$) and for the whole surface is given by $2d$ and by $4d$, respectively. For the neutral surface ($s=0$), $en_+ l^{(1)}$ is the contribution of the vacuum side ($z<0$) to the dipole moment $D(0)$, Eq. (2.7). Whereas this contribution is always positive, Friedel oscillations lead, for large r_s values, to negative contributions and very small values of the total dipole moment $D(0)$. Therefore, we take d (or $4d$) as a reasonable measure of the diffuseness of the surface and not the "dipole length" $D(\sigma)/(en_+ l^{(0)})$. The generalization of Eq. (3.1) to the surface of a metallic half-space without an infinite barrier is obvious.

Figure 6 shows on an enlarged scale the density profiles of Fig. 3 with the corresponding values of the diffuseness parameter d. Note that for all three profiles the density $n(z)$ assumes the value n_+ at the same position $z\approx 1.1$ Å. This would not be true for a rigid shift of the neutral profile by $s=\sigma/(en_+)$, indicated in Fig. 6 by a dashed vertical line, which would yield the same values of σ and would leave the values of $l^{(0)}$ and d unchanged. Further values of $l^{(0)}$ and d as a function of surface charge are given in Table I.

The correlation plot of Fig. 7 shows interesting characteristics of the density profile, notably of the low-density

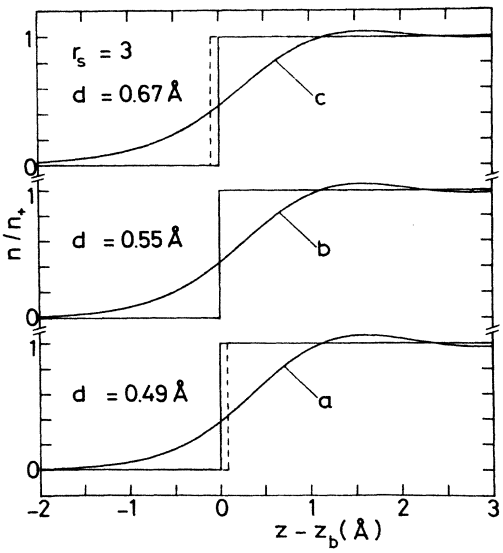

FIG. 6. Enlarged plot of the electron-density profiles from Fig. 3, with the diffuseness parameter d defined in Eq. (3.2). The dashed lines mark a shift by $s=\sigma/(en_+)$.

tail. All the symbols refer to self-consistently calculated profiles, the large symbols to neutral surfaces with different r_s values, and symbols of the same kind to surfaces with the same r_s value and different charges. Density profiles, which apart from a rigid shift differ only by length scale, e.g., $n(z)$ and $n(\alpha z-s)$, appear in this plot on the same straight line through the origin. With an exponential model for the tail region,

$$n(z)=\tfrac{1}{2}n_+ \exp[(z-s)/R]\ ,$$

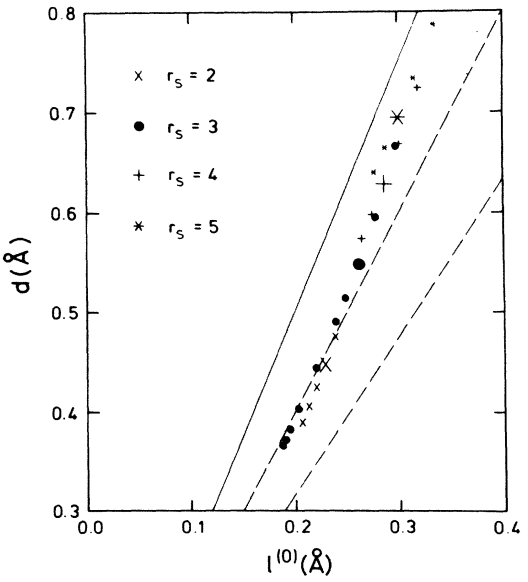

FIG. 7. Correlation plot of diffuseness parameters d and $l^{(0)}$ for the values of r_s and σ listed in Table I. The enlarged symbols refer to results for neutral systems. The straight lines indicate correlations for model density profiles discussed in the text.

one calculates from Eq. (3.1) (with $-a \to -\infty$) the dashed line in Fig. 7 with slope $d/l^{(0)}=2$. The frequently used infinite-barrier model (IBM) for a jellium half-space[19,20] with

$$n(z)=n_+\Theta(z)[1+3(Z\cos Z-\sin Z)/Z]\ , \tag{3.3}$$

where $Z=2zk_F$, $n_+=k_F^3/3\pi^2$, and the jellium edge is at $z_b=3\pi/8k_F$, yields, for arbitrary values of k_F, the dashed-dotted line shown in Fig. 7. The slope of this line is less than 2, indicating that the effective extent of the low-density tail for the IBM is smaller than that for the exponential model.

For $r_s=2$ the low-density tail of the uncharged surface apparently is well represented by an exponential model. Two points for positively charged surfaces with $r_s=2$ are also shown in Fig. 7. With increasing σ, the electron profile becomes steeper, the number of spilled-out electrons decreases, and the symbols occur at successively smaller values of $l^{(0)}$. The appearance of the symbols below the dashed line with slope 2 indicates that the low-density tails decrease faster than exponentially. The results for neutral and positively charged surfaces with $r_s=3$ (solid circles) show the same trend. In addition, one clearly sees the tendency of the points to converge for large σ values, indicating an ultimately rigid shift of the electron profile. The two results for negative surface charge and $r_s=3$ indicate a weaker than exponential decay of the electron density, so that the effective extent of the low-density tail increases.

The same trend is seen for the neutral surfaces as r_s increases. Although in the interior metal region the shape of the electron profile with increasing r_s becomes similar to that of the IBM, as has been demonstrated by Newns,[20] the effective extent of the low-density tail increases at the same time.[21]

Finally, we briefly consider the step model of Fig. 1(b) for the electron density $n(z)$, which is frequently used in optical model calculations. Well below the plasma frequency the optically induced charges reside in the surface region of reduced electron density (outside the jellium), and it seems reasonable to choose width w and electron density n_s of the surface layer so that $l^{(0)}$ and d, Eqs. (3.1) and (3.2), agree with the self-consistently calculated values. It is easily shown that this requires $d/l^{(0)}=n_+/2n_s$ and

$$l^{(0)}=(n_s/n_+)(1-n_s/n_+)\ ,$$

so that n_s/n_+ should be taken between $\frac{1}{5}$, corresponding to the solid line in Fig. 7, and $\frac{1}{4}$, corresponding to the dashed "exponential" line. For a neutral aluminum ($r_s=2$) surface this leads to $n_s=\frac{1}{4}n_+$ and $w=1.24$ Å. Different values ($n_s\approx 0.7n_+$, $w\approx 4$ Å) have been used to fit optical data near the plasma frequency,[7,16] where induced charges penetrate deeper into the metal and probe regions of higher electron density.

IV. SUMMARY

We have self-consistently calculated the electron density of a jellium slab containing about 8 occupied size-quantized eigenstates for various values of jellium density (r_s) and surface charge (σ). In the limit of small surface charge ($\sigma \to 0$), our slab results for the electron-density profile, induced charge density, etc. are in excellent agreement with those obtained by Lang and Kohn[3-5] for a jellium half-space. Our calculations cover the large range of surface charges accessible to experiments in electrolytic cells, which far exceeds the regime in which linear-response theory with respect to the applied static electric field is applicable.

We present results for two parameters which roughly characterize the induced charge-density profile, its width $\lambda(\sigma)$, and its center of mass $z_0(\sigma)$. The spread λ of the induced static charge density, which plays an important role for optical measurements on charged surfaces,[6-9,16,17] depends only weakly on the surface charge σ and is of the order of 1.5 Å (for $r_s=2$) to 2.5 Å (for $r_s=5$). The center of mass z_0 of the induced surface charge, which is important for static properties such as capacity or image-plane position, depends in a nonlinear manner on σ. For negative and small positive values of σ, z_0 lies in the low-density region on the vacuum side, and with increasing positive values of σ it approaches and eventually enters the jellium region inside the metal. Our calculation confirms recent variational results[12] for $z_0(\sigma)$ in the regime of moderate surface charges, but also indicates their limitations. Results of a recent evaluation of ellipsometry data on a charged gold surface[9] using a nonlocal theory[17] are consistent with our results, whereas those obtained with local optics[9] are not.

The shape of the total-electron-density profile is also studied as a function of surface charge. With increasing surface charge the electron-density profile becomes steeper. For very large values of σ the deformation saturates (owing to the Fermi pressure) and the profile is ultimately pushed rigidly into the jellium. As a quantitative characterization of the electron-density profile, two of its moments are given as functions of σ, and their correlation is discussed.

We hope that this work will be helpful for future investigations of optical properties of charged metal surfaces which, in our opinion, are not satisfactorily understood at present, although electroreflection now is a widely used tool in surface science.

ACKNOWLEDGMENTS

Financial support by the Deutsche Forschungsgemeinschaft through Sonderforschungsbereich 6 is gratefully acknowledged.

APPENDIX

We will describe here in detail how Eqs. (2.11) and (2.12) were solved numerically. Starting with an effective potential $v_{\rm eff}^{(1)}(z)$, we obtained the required energy eigenvalues ϵ_ν and the corresponding wave functions $\psi_\nu(z)$ by the integration method of Adams and Stoermer,[22] imposing the symmetry condition that either $\psi_\nu(z)$ or its derivative vanishes at $z=b$. The Fermi energy was evaluated from

$$\epsilon_F = \frac{\pi\hbar^2 n_+(b-s)/m + \int_{-a}^{b} dz \sum_\nu \Theta(\epsilon_F-\epsilon_\nu)\epsilon_\nu\psi_\nu^2(z)}{\int_{-a}^{b} dz \sum_\nu \Theta(\epsilon_F-\epsilon_\nu)\psi_\nu^2(z)} , \tag{A1}$$

and the density $n(z)$ from Eq. (2.11). From Eq. (2.14) we then calculated the new effective potential

$$\tilde{v}_{\rm eff}^{(2)}(z) = \mathcal{F}[v_{\rm eff}^{(1)}(z)] , \tag{A2}$$

which is a functional of the original one. Its fixed point is the required self-consistent effective potential $v_{\rm eff}(z)$.

To obtain fast convergence, we determined a linear approximation of $\mathcal{F}$ in the linear subspace of functions

$$v(z) = v_{\rm eff}^{(1)}(z) + \sum_{n=0}^{5} V_n u_n(z) , \tag{A3}$$

where $u_0(z) = v_{\rm eff}^{(1)}(z)$ is the input potential itself, four basis functions were chosen as Gaussians, and the last one was defined as zero at $z=b$, linear for $0<z<b$, and matched to a Gaussian for $z<0$. The equation for the new input potential reads

$$v_{\rm eff}^{(2)} = \mathcal{F}[v_{\rm eff}^{(1)}] + \eta^{-1} \sum_{n=0}^{5} V_n (\mathcal{F}[v_{\rm eff}^{(1)} + \eta u_n] - \mathcal{F}[v_{\rm eff}^{(1)}]) , \tag{A4}$$

$\eta = 0.02/r_s^2$. The coefficients $V_1, \ldots, V_5$ were calculated from a set of linear equations derived from the fixed-point equation in the subspace, and V_0 was taken as

$$V_0 = \tilde{v}_{\rm eff}^{(2)}(-a)/v_{\rm eff}^{(1)}(-a) - 1 . \tag{A5}$$

The self-consistent result was obtained after about five to eight iteration steps with an inaccuracy estimated by the integral

$$(a+b)^{-1}\epsilon_F^{-1} \int_{-a}^{b} dz \, | \, \mathcal{F}[v_{\rm eff}(z)] - v_{\rm eff}(z) \, | \ . \tag{A6}$$

This quantity was less than 0.2% for all our calculations.

A further estimate of numerical errors followed from the sum rule of Budd and Vannimenus,[18] which allows us to calculate the center of mass of the induced charge-density profile, $z_0(\sigma)$, defined in Eq. (2.8), alternatively by Eq. (2.10). The result is given in Table I, showing a deviation of less than 0.035 Å for all values of $z_0(\sigma)$.

[1]Preliminary results for a selected value of the bulk electron density have been published in advance in P. Gies and R. R. Gerhardts, Phys. Rev. B **31**, 6843 (1985).

[2]P. Hohenberg and W. Kohn, Phys. Rev. **136**, B864 (1964); W. Kohn and L. J. Sham, *ibid.* **140**, A1133 (1965).

[3]N. D. Lang, Solid State Commun. **7**, 1047 (1969); N. D. Lang and W. Kohn, Phys. Rev. B **1**, 4555 (1970).

[4]N. D. Lang and W. Kohn, Phys. Rev. B **3**, 1215 (1971).

[5]N. D. Lang and W. Kohn, Phys. Rev. B **7**, 3541 (1973).

[6]R. Kötz and D. M. Kolb, Z. Phys. Chem. (Frankfurt am Main) **112**, 69 (1978).

[7]F. Forstmann, K. Kempa, and D. M. Kolb, J. Electroanalyt. Chem. **150**, 241 (1983).

[8]A. Tadjeddine, D. M. Kolb, and R. Kötz, Surf. Sci. **101**, 277 (1980).

[9]F. Chao and M. Costa, Surf. Sci. **135**, 497 (1983); F. Chao, *ibid.* **157**, L328 (1985).

[10]A. K. Theophilou and A. Modinos, Phys. Rev. B **6**, 801 (1972).

[11]C. Warner, in *Thermionic Conversion Specialists Conference. San Diego, 1971* (Institute of Electrical and Electronics Engineers, New York, 1972), p. 170.

[12]W. Schmickler and D. Henderson, Phys. Rev. B **30**, 3081 (1984).

[13]V. I. Feldman, A. A. Kornyshev, and M. B. Partenskii, Solid State Commun. **53**, 157 (1985).

[14]K.-M. Ho, B. N. Harmon, and S. H. Liu, Phys. Rev. Lett. **44**, 1531 (1980).

[15]M. L. Cohen, M. Schlüter, J. R. Chelikowsky, and S. G. Louie, Phys. Rev. B **12**, 5575 (1975).

[16]F. Forstmann and R. R. Gerhardts, in *Festkörperprobleme (Advances in Solid State Physics)*, edited by J. Treusch (Vieweg, Braunschweig, 1982), Vol. XXII, p. 291.

[17]K. Kempa, Surf. Sci. **157**, L323 (1985).

[18]H. F. Budd and J. Vannimenus, Phys. Rev. B **12**, 509 (1975).

[19]R. R. Gerhardts and K. Kempa, Phys. Rev. B **30**, 5704 (1984).

[20]D. M. Newns, Phys. Rev. B **1**, 3304 (1970).

[21]P. J. Feibelman, Prog. Surf. Sci. **12**, 287 (1982).

[22]G. Jordan-Engeln and F. Reutter, *Formelsammlung zur numerischen Mathematik* (Bibliographisches Institut, Mannheim, 1981), p. 250.